VETOR

Understanding the role of human inter-provincial mobility on COVID-19 spread: a stochastic meta population model with time-dependent contact rates☆

Compreendendo o papel da mobilidade interprovincial humana na disseminação da COVID-19: um modelo metapopulacional estocástico com taxas de contacto dependentes do tempo

Paulo Joaquim[1], Daisuke Takahashi[2], Sansão A. Pedro [1†]

[1]*Universidade Eduardo Mondlane, Faculdade de Ciências - Maputo, Mozambique*
[2]*A. I. Systems Research Co., Ltd, Yoshidaushinomiya-cho, Sakyo-ku, Kyoto, Japan*
[†]**Corresponding author:** sansao.pedro@uem.ac.mz

Abstract

Epidemiological modeling that incorporates interprovincial mobility and time-varying contact rates is essential for elucidating the transmission dynamics of COVID-19. The migration of individuals between provinces and temporal fluctuations in contact rates shaped by social distancing directives are thought to be the pivotal factors influencing the spread of the disease. To investigate these variables, we constructed a stochastic metapopulation model consisting of 11 subpopulations, each delineated by a compartmental SEIAHRD submodel, to articulate COVID-19 transmission within the context of Mozambique. Inter-provincial mobility was quantified utilizing an origin-destination matrix derived from the radiation model. The interplay between human mobility and variability in contact rates was evaluated while testing three distinct scenarios: model without mobility; model with mobility and model with mobility and isolation of Maputo City. The model incorporating time-dependent contact rates demonstrated superior performance across all model scenarios. These results emphasize the significance of inter-regional mobility in shaping epidemic dynamics and underscore the effect of governmental interventions on fluctuations in contact rates. This investigation underscores the necessity for strategic mobility restrictions and adaptive measures in forthcoming epidemic control frameworks to enhance response efficacy and mitigate health and social repercussions.

Keywords

COVID-19 pandemic • Inter-provincial mobility • Stochastic metapopulation model • Radiation model • Time-dependent contact rates

Resumo

A modelação epidemiológica que incorpora mobilidade interprovincial e taxas de contacto variáveis no tempo é essencial para esclarecer a dinâmica de transmissão da COVID-19. A migração de indivíduos entre províncias e as flutuações temporais nas taxas de contacto moldadas por diretrizes de distanciamento social são consideradas factores essenciais que influenciam a disseminação da doença. Para investigar essas variáveis, construímos um modelo metapopulacional estocástico consistindo em 11 subpopulações, cada uma representada por um submodelo

☆This article is an extended version of the work presented at the Joint XXVII ENMC National Meeting on Computational Modeling, XV ECTM Meeting on Science and Technology of Materials,held in Ilhéus–Brazil,from October 1st to 4th,2024.

SEIAHRD compartimental, para investigar a transmissão da COVID-19 dentro do contexto de Moçambique. A mobilidade interprovincial foi quantificada utilizando uma matriz de origem-destino derivada do modelo de radiação. A interação entre mobilidade humana e variabilidade nas taxas de contacto foi avaliada testando três cenários distintos: modelo sem mobilidade; modelo com mobilidade e modelo com mobilidade e isolamento da Cidade de Maputo. O modelo que incorpora taxas de contacto dependentes do tempo demonstrou um desempenho superior em todos os cenários em relação ao modelo com taxa de contacto constante. Esses resultados enfatizam a importância da mobilidade inter-regional na formação da dinâmica epidêmica e ressaltam o efeito das intervenções governamentais nas flutuações nas taxas de contacto. Esta investigação ressalta a necessidade de restrições estratégicas de mobil idade e medidas adaptativas nos futuros programas de controle de epidemias para aumentar a eficácia da resposta e mitigar as repercussões sociais e de saúde pública.

Palavras-chave

Pandemia de COVID-19 • Mobilidade interprovincial • Modelo metapopulacional estocástico • Modelo de radiação • Taxas de contacto dependentes do tempo

1 Introduction

Since the start of the COVID-19 pandemic, the role of human mobility has been recognized extensively, establishing a correlation between reductions in mobility and the spread of the virus [1, 2, 3, 4, 5, 6]. Inter-regional mobility, defined as the relocation of individuals among different territories, significantly impacted the velocity and magnitude of viral transmission. Regions exhibiting high connectivity, characterized by a dense flow of individuals, witnessed a more rapid propagation of the virus, particularly during critical junctures of the pandemic [7, 8]. Grasping these mobility patterns was vital for forecasting outbreaks in various locales and for enacting targeted measures, including regional lockdowns and temporary travel prohibitions, aimed at alleviating the pandemic's repercussions and easing the strain on healthcare infrastructures [9, 2]. A general conclusion from these studies is that human mobility between regions contributes significantly to the initial transmission and spread of virus [10]. Since, reduction in mobility as a consequence of restrictive measures is shown to correlate with a reduction of new infections, it is important the to assess the long term effect of such social distancing measures in shaping the pattern of contact rates during an epidemic. Indeed, the relationship between contacts and mobility is expected to be time-varying [11]. During the pandemic, these rates exhibited considerable variability, shaped by social distancing directives and lockdowns, which temporarily curtailed interpersonal interactions and contributed to flattening the contagion curve [11]. Nevertheless, festive occasions and celebratory events precipitated elevated contact rates, frequently culminating in surges of cases [12]. By accounting for inter-provincial mobility and time-dependent contact rates, models can yield critical insights for policymakers, aiding in the formulation of more efficacious and timely containment strategies and optimizing resource distribution to manage the virus's transmission in a regionally nuanced manner [13].

One of the mathematical tools used to simultaneously integrate inter-regional mobility and disease transmission is the metapopulation modelling framework. Essentially, metapopulation models allows for the incorporation of spatial heterogeneity within a territory and the movement of individuals between subpopulations, providing a robust framework for analyzing how these dynamics impact disease transmission [14, 15]. Although it has long been known that human mobility is crucial for the predicting the epidemic and that mobility may also affect contact rates which in turn affect disease transmission [16], very few studies have assessed the composition effect of mobility and contact rates variability shaped by social distancing directives.

In the present work, we wish to expand our ealier study (presented at the Encontro Nacional de Modelagem Computacional, Ilheus 2024) to account for variations in social interactions across distinct temporal frames, such as weekdays versus weekends, holiday periods, and intervals of stringent restrictions. Since we have examined already the role of human mobility in the context of constant transmission rates, here our emphasis is on how infection rates variability, shaped by social distancing directives and lockdowns impacted the evolution of the pandemic in the context of human mobility. Our goal is to compare and contrast findings of an implementation with constant contact rates with one considering time-dependent infection rates. Following the same approach as in our previous work we attempt to understand and reproduce the spatial patern of COVID-19 pandemic in settings where data on people's movements is not readily available by implementing a metapopulation model with travel rates determined based on a radiation model. Such model is based on the assumption that population density dictates employment opportunities, hence, the predicted flux depends on the origin and destination populations and on the population of the region surrounding the origin location. We use the radiation model to simulate and generate the Origin-Destination matrix that captures resource disparities between provinces and their varying capacity in responding to the epidemics (for further discussion see [17, 1] and references therein). Since our goal is to examine the interplay between human mobility and the impact of social distancing directives and nation-wide lockdowns on the transmission rates over time we test the same model scenarios as in our previous work: scenario 1 model without mobility, scenario 2

model with mobility and scenario 3 model with mobility and isolation of Maputo City. We calibrate the model using cumulative case data from Mozambique [18] focusing on the period from the begining of the epidemic (March 22, 2020) to the end of the first wave (August 31, 2020). During calibration, we estimate four critical parameters for each province: the initial transmission rate (β_i^0), the incidence control parameter (ξ_i), the initial number of infectious individuals (I_i^0) and the intensity of the public interventions (σ_i). The later is implemented to account for population size variability in each location due to mobility.

For each scenario we compare the performance of the two models: model with constant contact rates and model with time-dependent contact rates. Our analysis shows that the model which integrates time-dependent contact rates generally surpasses the constant-rate model in performance, as demonstrated by consistently reduced RMSE values, especially in scenarios that incorporate interprovincial mobility. This observation suggests that temporal variations in contact rates, presumably influenced by intervention measures such as social distancing and movement restrictions, significantly contribute to the accurate representation of the transmission dynamics associated with COVID-19 in Mozambique. However, in the absence of mobility factors, the disparities in RMSE values between the two models are minimal, indicating that fluctuations in contact rates alone are inadequate to elucidate the observed data. This conclusion emphasizes the paramount significance of incorporating both time-dependent contact rates and mobility dynamics to attain a more precise depiction of disease transmission.

2 Material and Methods

2.1 Epidemic model for each subpopulation

To describe the transmission dynamics of COVID-19 in each province or subpopulation i, we implemented a stochastic and discrete compartmental epidemiological submodel **SEIAHRD**. Each compartment represents a state of individuals during the infection: **S** for susceptible, **E** for exposed, **I** for symptomatic infectious, **A** for asymptomatic infectious, **H** for hospitalized, **R** for recovered, and **D** for deceased. In each subpopulation i, the numberof individuals in each compartment at time t is indicated by $S_i(t)$, $E_i(t)$, $I_i(t)$, $A_i(t)$, $H_i(t)$, $R_i(t)$, and $D_i(t)$.

We assume no loss of immunity and no reinfection of recovered individuals. In a subpopulation i, the model initialization occurs at $START\_DAY_i$ ($t = START\_DAY_i$). Each simulation step lasts one day ($h = 1$). The number of individuals in each compartment each day depends on the previous day and the flows between compartments. Let $B_{kl}(t)$ be the number of transitions between compartments, with k as the origin and l as the destination. We use numerical labels: $S = 1$, $E = 2$, $I = 3$, $A = 4$, $H = 5$, $R = 6$, $D = 7$, described as follows: $B_{12}(t)$: new exposures after contact with infectious individuals; $B_{23}(t)$: new symptomatic cases; $B_{24}(t)$: new asymptomatic cases; $B_{35}(t)$: new hospitalizations; $B_{36}(t)$: recoveries after symptomatic infection; $B_{46}(t)$: recoveries after asymptomatic infection; $B_{56}(t)$ recoveries after hospitalization; $B_{57}(t)$: new deaths; corresponding to the schematic description shown in Fig. 1.

The transition between compartments is a stochastic process, modeled by a binomial distribution with a $seed = 11012024$ and where the number of trials equals the number of individuals in the current compartment. In each subpopulation we considered a non constant transmission rate, given by

$$\beta_i(t) = \begin{cases} \beta_i^0\,, & \text{if } 0 \le t \le t_{eff} \\ \beta_i^0 exp\left(-\sigma_i\left(t - t_{eff}\right)\right), & \text{if } t_{eff} < t \end{cases} \tag{1}$$

where β_i^0 is the initial infection rate, t_{eff} corresponds to the day when the public measures take effect and σ_i is the rate at which they take effect [19].

It is assumed that transmission occurs through close contact between susceptible and infectious individuals, with a probability $\lambda_i(t)$, called the force of infection, given by

$$\lambda_i(t) = 1 - [1 - \beta_i(\xi + (1 - \xi)/N_i)]^{N_i^+}, \tag{2}$$

where β_i is the infection rate, N_i is the total number of individuals in subpopulation i, $N_i^+ = I_i(t) + A_i(t) + H_i(t)$, and ξ controls the incidence: $\xi = 0$ for standard and $\xi = 1$ for density-dependent incidence [20].

Our model is along the lines of [21], and the stochastic compartmental model in discrete time for COVID-19

assumes the following form

$$\begin{aligned} S_i(t+h) &= S_i(t) - B_{12}(t) \\ E_i(t+h) &= E_i(t) + B_{12}(t) - B_{23}(t) - B_{24}(t) \\ I_i(t+h) &= I_i(t) + B_{23}(t) - B_{35}(t) - B_{36}(t) \\ A_i(t+h) &= A_i(t) + B_{24}(t) - B_{46}(t) \\ H_i(t+h) &= H_i(t) + B_{35}(t) - B_{56}(t) - B_{57}(t) \\ R_i(t+h) &= R_i(t) + B_{36}(t) + B_{46}(t) + B_{56}(t) \\ D_i(t+h) &= D_i(t) + B_{57}(t), \end{aligned} \tag{3}$$

where

$$B_{12}(t) \sim \text{Bin}(S_i(t), P_{12}(t)), \quad B_{23}(t) \sim \text{Bin}(E_i(t), P_{23}), \quad B_{24}(t) \sim \text{Bin}(E_i(t), P_{24}), \quad B_{35}(t) \sim \text{Bin}(I_i(t), P_{35}),$$
$$B_{36}(t) \sim \text{Bin}(I_i(t), P_{36}), \quad B_{46}(t) \sim \text{Bin}(A_i(t), P_{46}), \quad B_{56}(t) \sim \text{Bin}(H_i(t), P_{56}), \quad B_{57}(t) \sim \text{Bin}(H_i(t), P_{57}).$$

The random variables above involve binomial distributions B(n, p) with the following probabilities: $P_{12}(t) = \lambda_i(t)$, where $\lambda_i(t)$ is the force of infection; $P_{23} = \alpha(1-\rho)$, where α is the incubation rate and $(1-\rho)$ is the proportion of symptomatic infectious individuals; $P_{24} = \alpha\rho$, where ρ is the proportion of asymptomatic infectious individuals; $P_{35} = \gamma_1\mu$, where γ_1 is the rate at which symptomatic individuals become recovered and μ is the proportion of hospitalized individuals; $P_{36} = \gamma_1(1-\mu)$; $P_{46} = \gamma_2$, where γ_2 is the rate at which asymptomatic individuals become recovered; $P_{56} = \gamma_3(1-\omega)$, where γ_3 is the rate at which hospitalized individuals become recovered and $1-\omega$ is the proportion of individuals recovered after hospitalization; $P_{57} = \gamma_3\omega$, where ω is the proportion of individuals declared deceased after hospitalization.

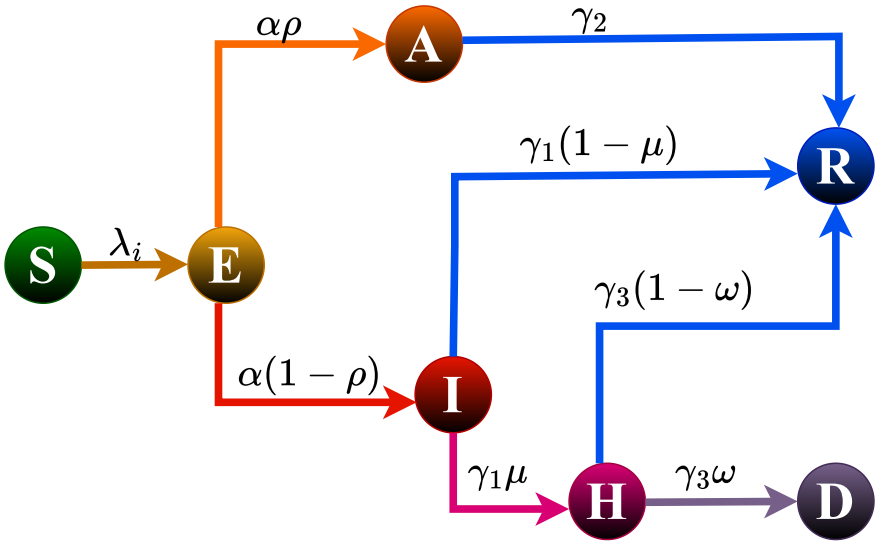

Figure 1: Transfer diagram of the **SEIAHRD** epidemic model in each node.

2.2 Data and human mobility estimation

Nation-wide COVID-19 lockdown restrictions in Mozambique were implemented since the notification of the first COVID-19 case on 22 March 2020. However, mobility between regions such as provinces was never restricted. The main goal of this sudy is to use a metapopulation modelling framework for studying and understanding the effect of human mobility on the spread of COVID-19 between provinces while accounting for contact rates variability, shaped by social distancing directives and lockdowns. In recent days mobility flows between regions are commonly estimated from mobile-phone records. However, such daily mobility data provided by mobile phones are not readily and publicly available in low-income countries such as Mozambique. In this case, in order to quantify mobility between provinces we use alternative models to determine the daily populattion flows.

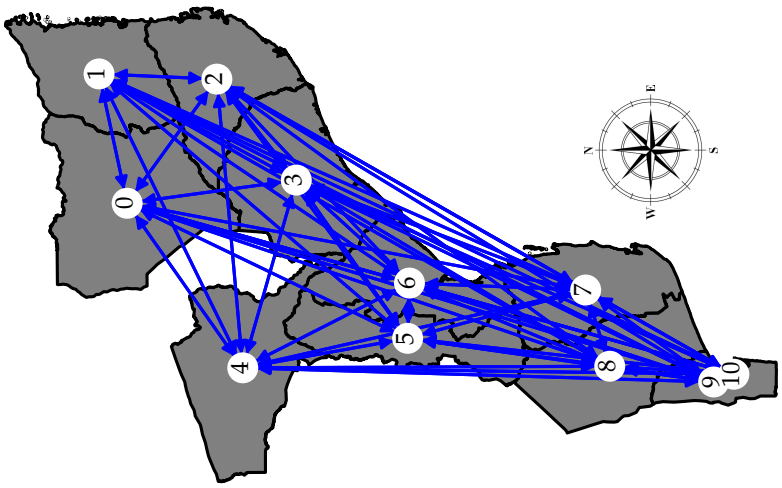

Figure 2: Synthetic interprovincial mobility network, where **0** represents Niassa Province, **1** represents Cabo Delgado Province, **2** represents Nampula Province, **3** represents Zambézia Province, **4** represents Tete Province, **5** represents Manica Province, **6** represents Sofala Province, **7** represents Inhambane Province, **8** represents Gaza Province, **9** represents Maputo Province, and finally **10** represents the Maputo City.

One of the most commonly used models is the gravity model, which is based on empirical evidence that the commuting between two places is proportional to the product of the populations and inversely proportional to the distance between them [22]. However, the gravity model has limitations, such as the lack of a rigorous derivation, the use of various distance functions, and the need for previous traffic data to fit the parameters [23]. These limitations can be overcomed by the radiation model, which reproduces commuting movements without the need for parameters or fitting to existing data, making it ideal for generating a synthetic commuting network in the absence of empirical data [24]. The model is based on a stochastic decision process, determining the daily commuting fluxes of individuals between the eleven provinces of Mozambique.

Therefore, to compute the origin-destination matrix for interprovincial connections compatible with empirical data collected through the interprovincial road transport system network, we used the radiation model based on population data from the Instituto Nacional de Estatistica. To simulate mobility between provinces, we built a synthetic network, composed of V nodes and M connections, where the nodes represent the center of each Mozambican province and the connections symbolize the movement of individuals between them, as illustrated in Fig. 2.

The mobility is regulated by the parameter τ, known as the mobility coefficient, and the weights T_{ij} of connections between subpopulations [25]. Thus, each weight T_{ij} corresponds to an entry in the OD matrix, generated by simulating the radiation model implemented in the Python library Sciki-mobility, as developed by [26]. Proposed by [23], the radiation model is expressed as

$$\langle T_{ij} \rangle = T_i \frac{N_i N_j}{(N_i + K_{ij})(N_i + N_j + K_{ij})}, \tag{4}$$

where N_i is the population in the originating province i, N_j is the population in the destination province j, K_{ij} is the total population within the circle of radius centered at i excluding i and j, and $\sum_{j \neq i} T_{ij} \equiv T_i$ represents the total travelers originating from i, proportional to the local population.

According to [24], the OD matrix resulting from the simulation represents the estimated daily displacement flows across the entire country. The resulting OD matrix from our simulation is presented in Table 1 below.

Table 1: Values of daily flows across the entire country.

		DESTINATION										
		0	**1**	**2**	**3**	**4**	**5**	**6**	**7**	**8**	**9**	**10**
ORIGIN	**0**	0	986	119	74	24	13	17	16	12	46	23
	1	396	0	1547	509	172	68	145	85	62	267	229
	2	111	1513	0	399	66	32	77	45	39	139	113
	3	196	214	1476	0	150	127	401	56	58	235	180
	4	61	73	89	310	0	626	434	30	21	81	43
	5	2	0	1	45	196	0	624	67	15	62	21
	6	16	1	54	515	66	646	0	97	42	111	55
	7	0	3	1	3	2	0	2	0	868	710	115
	8	0	2	3	1	0	2	1	897	0	779	129
	9	76	184	172	223	117	82	122	128	148	0	12447
	10	838	2275	1797	2471	1307	985	1400	1753	2006	21166	0

Movements between subpopulations are random processes and connections between provinces depend on the mobility flow of susceptible **S**, exposed **E**, infectious hosts, **A** and **I**, and recovered, **R**. Furthermore, since there were no mobility restrictions between provinces at the time, we assume that the movement of exposed, and infectious and recovered individuals is the same as the movement of susceptible individuals. Using multinomial sampling across the permitted compartments (**S, E, I, A, R**), with the number of trials being determined by the individuals available in each compartment and the probability

$$p_{ij} = \frac{\tau \sum_j T_{ij}}{N_i(0)}, \tag{5}$$

where τ is the mobility coefficient, τT_{ij} represents the expected number of travelers from i to j, and $N_i(0)$ is the initial number of individuals in subpopulation i.

Only individuals from compartment S can travel to another province $j \neq i$ before $START\_DAY_j$. For each compartment X ({S, E, I, A, R}) in subpopulation i and time t, after determining $X_{ij}(t)$, the number of individuals traveling from i to j, $\sum_j X_{ij}(t)$ represents the total number of individuals in compartment X leaving subpopulation i for other subpopulations j. On the other hand, $\sum_j X_{ji}$ indicates the total number of individuals entering i from different subpopulations j. In each compartment X, an individual has the possibility to move from subpopulation i to one of $J = 10$ other subpopulations. Thus, this process can be expressed as a multinomial distribution:

$$(X_{i1}(t), \dots, X_{iJ}(t)) \sim \text{Multinomial}\,(X_i(t), J, p_{i1}, \dots, p_{iJ}) \tag{6}$$

where $(p_{i1}, \dots, p_{iJ})$ are given by each row of the transition matrix ilustrated in Fig. 3.

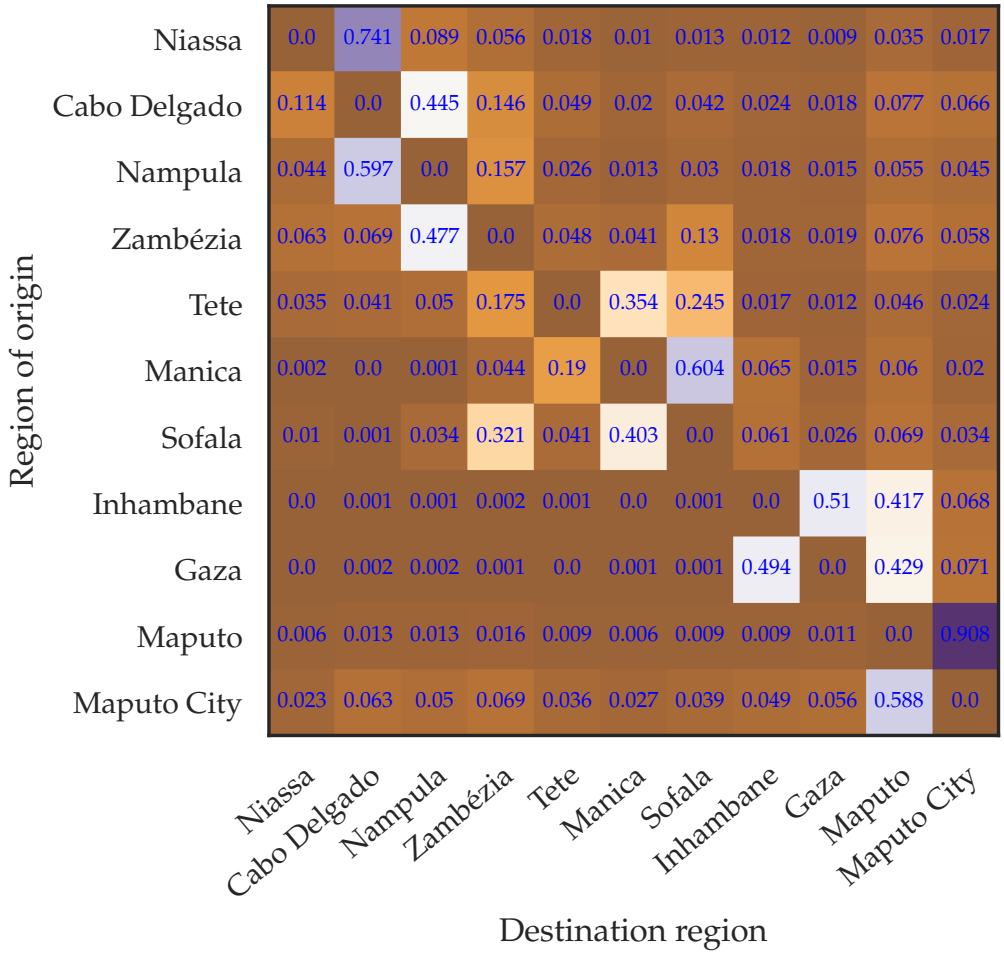

Figure 3: The probability matrix (p) computed using the Eq. (5), with $\tau = 1$. p_{ij} is the probability that an individual who came from one of the 11 regions to region j, originated from region i.

2.3 Metapopulation model

Using notation defined in the previous section, we extend model (3) by incorporating interprovincial mobility terms, leading to the following metapopulation model for COVID-19 transmission, described by system (7),

$$\begin{aligned}
S_i(t+h) &= S_i(t) - B_{12}(t) - \sum_j S_{ij}(t) + \sum_j S_{ji}(t) \\
E_i(t+h) &= E_i(t) + B_{12}(t) - B_{23}(t) - B_{24}(t) - \sum_j E_{ij}(t) + \sum_j E_{ji}(t) \\
I_i(t+h) &= I_i(t) + B_{23}(t) - B_{35}(t) - B_{36}(t) - \sum_j I_{ij}(t) + \sum_j I_{ji}(t) \\
A_i(t+h) &= A_i(t) + B_{24}(t) - B_{46}(t) - \sum_j A_{ij}(t) + \sum_j A_{ji}(t) \\
H_i(t+h) &= H_i(t) + B_{35}(t) - B_{56}(t) - B_{57}(t) \\
R_i(t+h) &= R_i(t) + B_{36}(t) + B_{46}(t) + B_{56}(t) - \sum_j R_{ij}(t) + \sum_j R_{ji}(t) \\
D_i(t+h) &= D_i(t) + B_{57}(t)
\end{aligned} \tag{7}$$

Though, starting from model (7), we can revert to model (3) simply by setting $\tau = 0$ in Eq. (5), thereby eliminating all terms representing interprovincial mobility.

Based on the description so far, the simulation process of our computational model is as the following: in each simulation step, transmission rules are applied in each province, followed by updating the number of individuals

in each state. Subsequently, mobility rules are implemented to determine how many individuals travel through each connection. After calculating all flows, the number of individuals in each state across all provinces is updated. According to [25], the results are independent of the order in which visits to subpopulations are made for performing calculations.

2.4 Model calibration

Table 2: Non and calibrated parameter values by province.

Parameter	Definition	Value	Source	Province
α	Incubation rate of Exposed individuals	$1/5.1\ days^{-1}$	[27]	
ρ	Proportion of Asymptomatic individuals	0.05	[28]	
γ_1	Recovery rate of Symptomatic Infectious individuals	$1/10\ days^{-1}$	[17]	
γ_2	Recovery rate of Asymptomatic Infectious individuals	$1/9.5\ days^{-1}$	[29]	All
γ_3	Recovery rate of Hospitalized infectious individuals	$1/18.1\ days^{-1}$	[29]	
μ	Proportion of Hospitalized Infectious individuals	0.05	[17]	
ω	Proportion of declared Deaths	0.2	[17]	
τ	Mobility coefficient	$[0, 1]$	[25]	
t_{eff}	First day of the public interventions	26	[18]	
$START\_DAY_0$	Notification date of the 1^{st} case	67 (28/05/20)	[18]	Niassa
$START\_DAY_1$	Notification date of the 1^{st} case	17 (08/04/20)	[18]	Cabo Delgado
$START\_DAY_2$	Notification date of the 1^{st} case	63 (24/05/20)	[18]	Nampula
$START\_DAY_3$	Notification date of the 1^{st} case	64 (25/05/20)	[18]	Zambézia
$START\_DAY_4$	Notification date of the 1^{st} case	56 (17/05/20)	[18]	Tete
$START\_DAY_5$	Notification date of the 1^{st} case	56 (17/05/20)	[18]	Manica
$START\_DAY_6$	Notification date of the 1^{st} case	50 (11/05/20)	[18]	Sofala
$START\_DAY_7$	Notification date of the 1^{st} case	50 (11/05/20)	[18]	Inhambane
$START\_DAY_8$	Notification date of the 1^{st} case	59 (20/05/20)	[18]	Gaza
$START\_DAY_9$	Notification date of the 1^{st} case	25 (16/04/20)	[18]	Maputo
$START\_DAY_{10}$	Notification date of the 1^{st} case	0 (22/03/20)	[18]	Maputo City
β_0^0	Transmission rate	$0.0004338908\ days^{-1}$	Calibrated	Niassa
β_0^0	Transmission rate	$0.0006562742\ days^{-1}$	Calibrated	Cabo Delgado
β_2^0	Transmission rate	$0.0005244815\ days^{-1}$	Calibrated	Nampula
β_3^0	Transmission rate	$0.0003171671\ days^{-1}$	Calibrated	Zambézia
β_4^0	Transmission rate	$0.0003265976\ days^{-1}$	Calibrated	Tete
β_5^0	Transmission rate	$0.0000117325\ days^{-1}$	Calibrated	Manica
β_6^0	Transmission rate	$0.0004809578\ days^{-1}$	Calibrated	Sofala
β_7^0	Transmission rate	$0.0000198328\ days^{-1}$	Calibrated	Inhambane
β_8^0	Transmission rate	$0.0004270757\ days^{-1}$	Calibrated	Gaza
β_9^0	Transmission rate	$0.0003929000\ days^{-1}$	Calibrated	Maputo
β_{10}^0	Transmission rate	$0.0001855232\ days^{-1}$	Calibrated	Maputo City
ξ_0	Control parameter of the incidence function	0.039139475	Calibrated	Niassa
ξ_1	Control parameter of the incidence function	0.021465552	Calibrated	Cabo Delgado
ξ_2	Control parameter of the incidence function	0.024353480	Calibrated	Nampula
ξ_3	Control parameter of the incidence function	0.009317492	Calibrated	Zambézia
ξ_4	Control parameter of the incidence function	0.014096507	Calibrated	Tete
ξ_5	Control parameter of the incidence function	0.000959269	Calibrated	Manica
ξ_6	Control parameter of the incidence function	0.008683023	Calibrated	Sofala
ξ_7	Control parameter of the incidence function	0.008554156	Calibrated	Inhambane
ξ_8	Control parameter of the incidence function	0.021586286	Calibrated	Gaza
ξ_9	Control parameter of the incidence function	0.053554408	Calibrated	Maputo
ξ_{10}	Control parameter of the incidence function	0.077848052	Calibrated	Maputo City
I_0^0	Initial number of Infectious individuals	6	Calibrated	Niassa
I_1^0	Initial number of Infectious individuals	9	Calibrated	Cabo Delgado
I_2^0	Initial number of Infectious individuals	8	Calibrated	Nampula
I_3^0	Initial number of Infectious individuals	5	Calibrated	Zambézia
I_4^0	Initial number of Infectious individuals	6	Calibrated	Tete
I_5^0	Initial number of Infectious individuals	7	Calibrated	Manica
I_6^0	Initial number of Infectious individuals	8	Calibrated	Sofala
I_7^0	Initial number of Infectious individuals	5	Calibrated	Inhambane
I_8^0	Initial number of Infectious individuals	4	Calibrated	Gaza
I_9^0	Initial number of Infectious individuals	5	Calibrated	Maputo
I_{10}^0	Initial number of Infectious individuals	5	Calibrated	Maputo City
σ_0	Intensity of the public interventions	0.142309933	Calibrated	Niassa
σ_1	Intensity of the public interventions	0.126971885	Calibrated	Cabo Delgado
σ_2	Intensity of the public interventions	0.124929708	Calibrated	Nampula
σ_3	Intensity of the public interventions	0.119616215	Calibrated	Zambézia
σ_4	Intensity of the public interventions	0.140194250	Calibrated	Tete
σ_5	Intensity of the public interventions	0.344212494	Calibrated	Manica
σ_6	Intensity of the public interventions	0.108525353	Calibrated	Sofala
σ_7	Intensity of the public interventions	0.140509810	Calibrated	Inhambane
σ_8	Intensity of the public interventions	0.121579276	Calibrated	Gaza
σ_9	Intensity of the public interventions	0.129062435	Calibrated	Maputo
σ_{10}	Intensity of the public interventions	0.108669405	Calibrated	Maputo City

In the model calibration process, we used an effective population and the cumulative case data recorded by [18] between March and August 2020. For each province, the effective population corresponds to a proportion of the inhabitants from the districts with the highest number of cumulative cases in the first wave of COVID-19 infections in Mozambique according to the data from the IV General Population Census of 2017. To perform the calibration, we used a combination of the Hyperband and Tree-Structured Parzen Estimator (TPE) algorithms, both implemented in the Python library Optuna, developed by [30]. The performance of the calibrated parameters was evaluated using the root mean square error as a metric, given by the Eq. 8

$$RMSE = \sqrt{\frac{\sum_{t=1}^{T}(y_t - \hat{y}_t)^2}{T}}, \tag{8}$$

where T represents the calibration period, y_t are the cummulative case records and $\hat{y}_t$ are the cummulative cases generated by the model.

It is important to mention that for each province, four parameters were adjusted: the initial transmission rate (β_i^0), the incidence control parameter (ξ_i), the initial number infectious individuals (I_i^0) and the intensity of the public interventions (σ_i). These parameters are crucial for our study because, during the first wave of COVID-19 infections in Mozambique, a heterogeneity in the dynamics of virus transmission was observed between provinces. It is presumed that this was caused by differences in the magnitude of various factors, including population density, geographic connectivity, social behavior, and adherence to public health protection measures in each province. A full list of parameter definitions, baseline values, and literature sources is presented in Table 2 above.

3 Results

Sensitivity analysis

For each province, we conducted a sensitivity analysis of the four calibrated parameters. This analysis reveals how the variation in parameters and initial conditions of the mathematical model affects a quantity of interest [31]. Sensitivity Sobol indices can be classified into first-order indices, second-order indices, and total-order indices [32]. In this study, we investigated the total-order Sobol index, which measures the contribution of a parameter to the variance of our quantity of interest (the cumulative number of cases) in each province, including both its first-order effects and all higher-order interactions. To assess the index, it is imperative to calculate the variance attributed to a parameter by evaluating its singular impact alongside its synergistic interactions with other parameters across all conceivable interactions. To carry out this process, we first defined a range of $[-30\%, +30\%]$ for each calibrated parameter and then used the Python library SALib, as implemented by [32], to obtain the sensitivity index values.

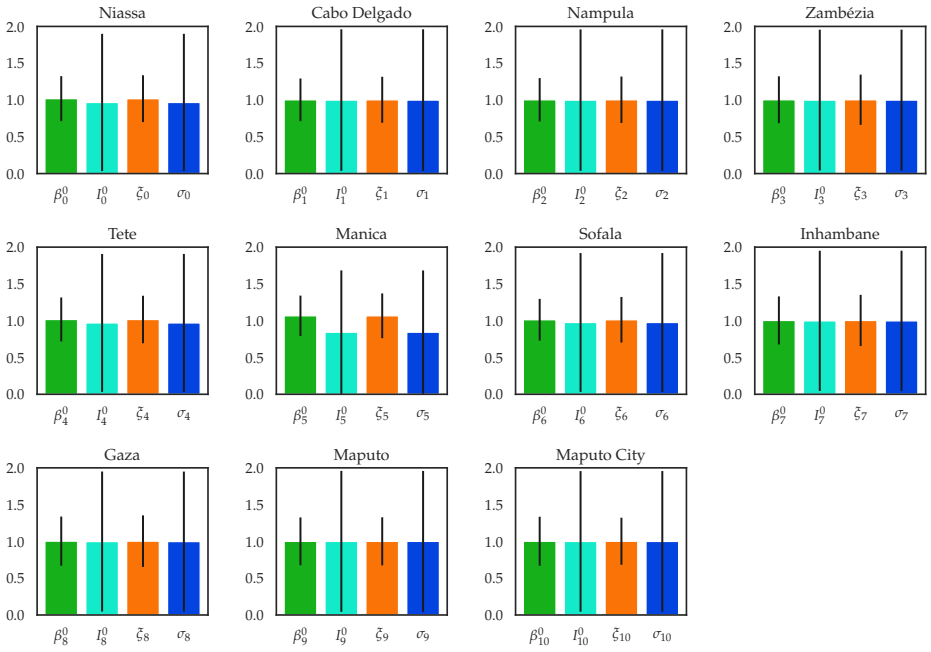

Figure 4: Total-order Sobol indices of the number of cummulative cases for each Mozambican province. The length of the bars indicate the mean values, while the thinner black lines display the 95% confidence interval.

The results are presented in Figure 4. In all provinces except for Manica, the mean values of the total-order Sobol indices for all four parameters are close to 1. This indicates that, in these provinces, all four parameters interactively contribute equally to the uncertainty in the model's output [33]. Collectively, they affect the variance of the cumulative case count, with the influence of each parameter being inherently intertwined with its interactions with the other parameters, thereby highlighting the imperative of accounting for both individual and higher-order contributions to the model's uncertainty.

Furthermore, Figure 4 elucidates broader 95%confidence intervals for the indices of the parameters I_i^0 and σ_i, thereby indicating a heightened degree of imprecision in the estimations of these parameters' indices. This observation implies that these particular parameters contribute to increased levels of variability and uncertainty within the model's predictive outcomes. Such variability may stem from the intricate, non-linear interactions between these parameters and other variables within the model, or could arise from constraints inherent in the data or the assumptions employed to ascertain their contributions. Elucidating these elements could facilitate the refinement of the model and mitigate uncertainty.

Model predictions

To test the performance of the metapopulation model in capturing the evolution pattern of the first wave of COVID-19 epidemic in Mozambique when variability of contact rates shaped by social distancing directives and nation-wide lockdowns is taken into account we compare two models: model 1, the model with constant rates and model 2, the model with time dependent infection rates. Since model 1 is the model considered in our previous work, here our emphasis is on determining how the interplay between mobility and time dependent infection rates improves the model in reproducing the observations. We consider the same simulation period as in the previous work from March 22, 2020, to November 30, 2020. During this interval, we used the first 162 days (from March 22, 2020, to August 31, 2020) to adjust the model and the subsequent 91 days to predict the model's behavior. The occurrence of the peak between August and October 2020, as well as the exponential growth phase of the first wave, were determining factors in choosing the model adjustment period.

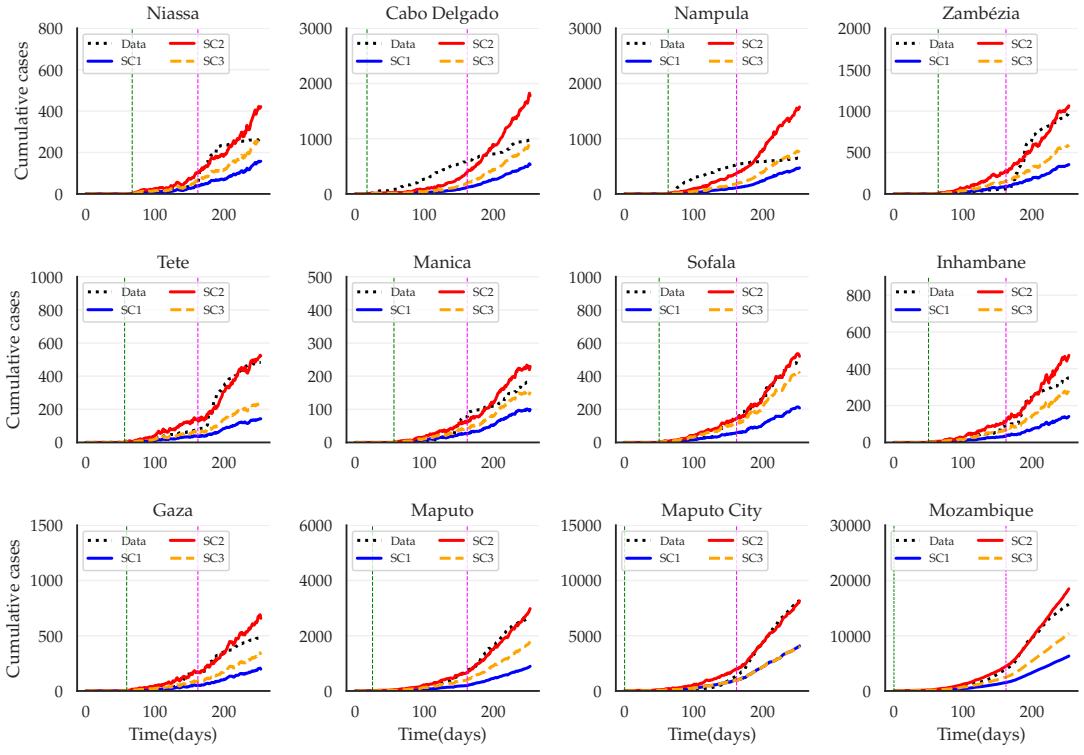

Figure 5: Cumulative case data (black dots) and model fits for each province, with national data in the last row of column 3. The blue curve represents the model without mobility off ($\tau = 0$), the red curve represents the metapopulation model with mobility ($\tau = 1$), and the dashed orange curve represents the model with mobility and isolation of Maputo City ($\tau = 1, T_{10j} = 0 = T_{j10}$). The green vertical line denotes the model initialization date ($t = START\_DAY_i$), and the magenta vertical line marks the end of the fit and the start of predictions (day 162). The interquartile range for the red curve is highlighted in light red.

Fig. 5 shows the fit of the **SEIAHRD** model with time-dependent transmission rates in three scenarios: model without mobility ($\tau = 0$), model with mobility ($\tau = 1$) and model with mobility and isolation of Maputo City. We observe that only the metapopulation model curves are close to each other and trail the data points with a satisfactory level of accuracy. The observed divergence within the prediction interval, wherein solely the metapopulation model incorporating mobility corresponds with the trajectory of the actual data, indicates that human movement across provinces markedly impacted the transmission patterns during the initial wave of the pandemic. This outcome accentuates the pivotal significance of interprovincial mobility in precisely elucidating the dynamics of the COVID-19 epidemic in Mozambique. The failure of the model devoid of mobility, along with the model that isolates Maputo City, to replicate the observed trends within the prediction interval underscores the necessity of integrating realistic mobility patterns within epidemic models. In the absence of mobility, the spatial interconnectivity and circulation of individuals, which serve as critical drivers of viral propagation, are neglected, culminating in overly simplified projections. Likewise, the isolation of Maputo City, although theoretically a sound containment strategy, may fail to accurately represent the practical dynamics of mobility restrictions and their enforcement, potentially resulting in discrepancies within the model's predictive efficacy.

These results are in agreement with previous research [34, 11] that highlight the complex interplay between mobility and transmission rates, although not ignoring other factors such as risk perception that do affect both mobility and contacts, therefore, potentially affecting their mutual relationship [11]. They also exemplify the imperative of employing time-dependent transmission rates, as static rates inadequately capture the temporal variability engendered by intervention measures and behavioral adaptations. Other findings [35] suggest that these parameters facilitated the analysis of how SARS-CoV-2 traversed regional boundaries and how interventions such as quarantines, travel restrictions, and social distancing measures influenced infection prevalence. To ilustrate the critical role of the interplay between these two factors, for each simulation scenario mentioned above, we compare the performance of the two models by computing the normalized Root Mean Square Error (RMSE) between the model's predicted data and the actual cumulative cases, using the Python library Scikit-learn, developed by [36]. For the case of the model without mobility (i.e. scenario SC1) the findings of this assessement are depicted in Fig. 6, which contrasts the Root Mean Square Error (RMSE) values for a model that is based on constant contact rates (represented by grey bars), against the same model with time-dependent contact rates (illustrated by dark blue bars). The results suggest that the model integrating time-dependent contact rates attained marginally lower RMSE values in comparison to the model based on constant contact rates. We note however that the differences in RMSE values between the two models are not substancial. A plausible rationale for this observation resides in the fact that in the abscence of inter-regional mobility, variability in contact rates alone shaped by social distancing directives is insuffcient to explain the dynamics of the pandemics. Another important key finding that is ilustrated Fig. 6 is that the upgrade from model with no mobility to the model with mobility has significantly improved the model fit and forecast quality. The results indicates that the model utilizing time-dependent contact rates consistently yielded inferior RMSE values in comparison to the model predicated on constant rates. It is particularly noteworthy that, with the exception of the provinces of Cabo Delgado and Nampula, the discrepancies in RMSE between the two models are statistically significant, thereby leading to the inference that the model with time-dependent contact rates exhibited superior efficacy. Futhermore, the third column ilustrating the isolation of Maputo City indicates the role of this region in shaping the pattern of the epidemic in the rest parts of the country, highlighting the role of strongly connected regions.

These outcomes robustly substantiate our hypothesis that contact rates within each province of Mozambique exhibit temporal fluctuations. Such temporal variability is likely shaped by the intervention strategies enacted by governmental authorities during the initial wave of COVID-19 infections. These interventions exerted a direct influence on the transmission rates of COVID-19, as demonstrated by earlier research [34, 11]. Moreover, the gradual exponential increase observed in cumulative case counts throughout the first wave in Mozambique [28] reinforces the efficacy of these interventions.

The findings emphasize the significance of incorporating time-dependent dynamics in contact rates when conducting epidemic modeling, as this methodology captures the intricate effects of intervention strategies and provides a more precise representation of disease transmission patterns.

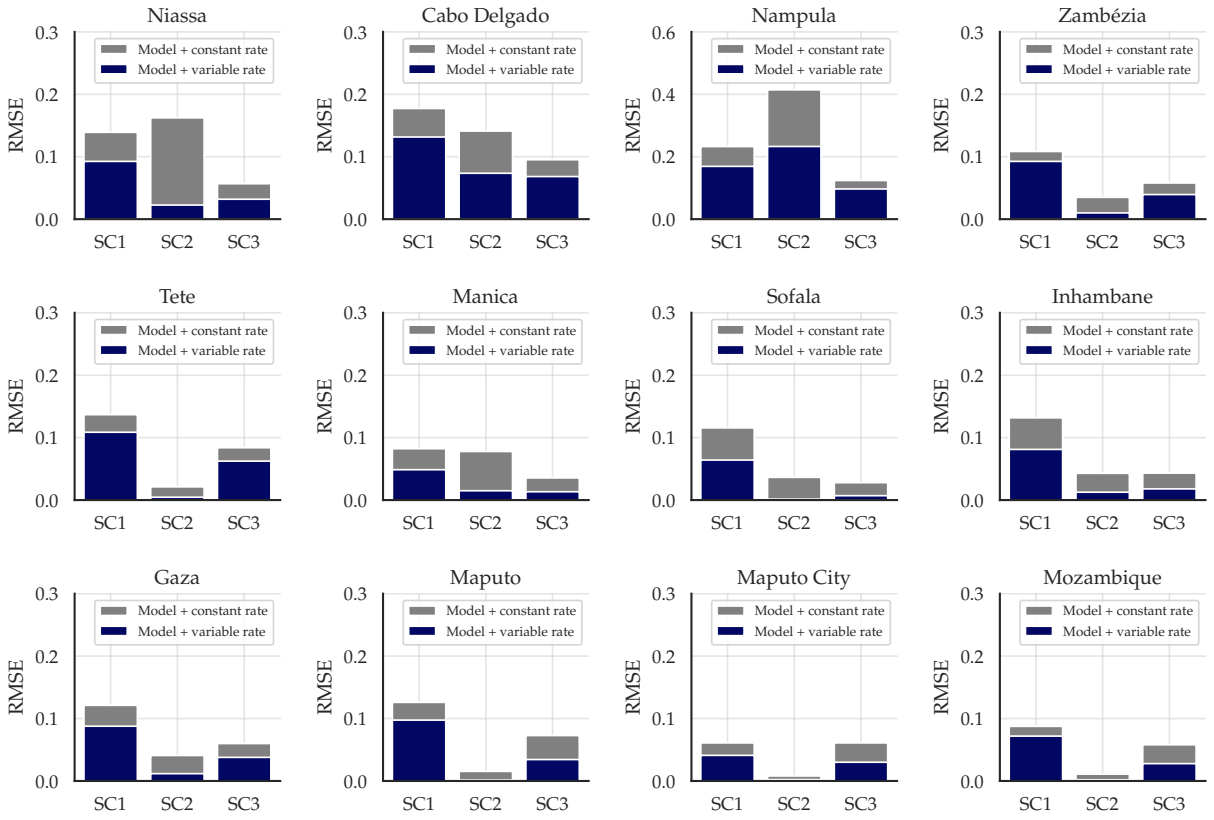

Figure 6: Comparison of the Root Mean Square Error (RMSE) between model 1 (constant contact rates) and model 2 (time-dependent contact rates) for the thee simualtion scenarios: without mobility (SC1), with mobility (SC2) and with mobility and isolation of Maputo City (SC3), presented by province. The gray bars represent the RMSE of the model 1, while the dark blue bars represent the RMSE of the model 2.

4 Discussion and Conclusion

Here we compared two models for assessing the role of human mobility in the dynamics of COVID-19 epidemic in Mozambique. Using a model with constant transmission rates, in our previous work [37] we found that in the absence of mobility among provinces the model was unable to predict the epidemic curve during the first wave. Instead, the most accurate quantitative description of the observations in each province was attained when mobility was activated. It has long been known that human mobility is crucial at the beginning stages of an epidemic, when the infection is seeded in various locations [35, 2, 16]. Furthermore, mobility may also affect contact rates which in turn affect disease transmission [16]. Therefore, we now extended the analysis presented in the previous work with the intention to evaluate if incorporating the variability of contact rates shaped by social distancing directives and nationwide lockdowns improves the performance of the mobility model in predicting the observations. This is achieved by modifying the force of infection to include changes in the infection rate according to the cronology of implemented interventions. Since the goal was to assess the performance of the mobility model with time dependent contact rates we tested the same simulation scenarios as in the previous work: Scenario 1, a model without mobility; Scenario 2, a model with mobility; and Scenario 3, a model with mobility and isolation of Maputo City. The simulation results revelead that Scenario 2 was the most effective in capturing and reproducing the pattern of cumulative COVID-19 cases in the country. In contrast, Scenarios 1 and 3 demonstrated a slowdown in exponential growth, resulting in significant reductions in the cumulative number of cases and in higher RMSE compared to Scenario 2. These findings highlight that during the first wave of the COVID-19 pandemic, interprovincial mobility was one of the main factors driving the spread of the virus, which started in Maputo City to other regions of the country. Furthermore, the results indicated that the control measures implemented by government authorities significantly influenced the variability of contact rates across provinces over time, suggesting that information on the influence of inter-regional mobility on disease spread is useful for regional policymakers. Based on the results of this study, we conclude that interprovincial mobility should be prioritized in the planning of effective intervention strategies for future epidemics similar to COVID-19 and how such interventions shape the nature of contact rates. In particular, the connectivity

of Maputo City with other provinces emerges as a critical aspect requiring the attention of policymakers. Focusing on these factors could optimize control measures, enhance the effectiveness of epidemic responses, and minimize the health and socio economic impact of the disease on communities. The sensitivty analysis on key four model parameters: initial transmission rate, incidence control parameter, intensity of interventions and initial number of infectious individuals indicated that all parameters interactively and strongly contributed equally to model output. Of particular interest is the estimate of initial number of infected individuals to initialize the epidemic in each location, which varied significantly from the figures reported by government authorities. Such differences stem from a number of factors including the incubating period and asymptomatic cases for young health people, late inspection and delayed quarantine policies and limited testing infrastructure.

For subsequent research endeavors, we propose an extension of our model to incorporate the synchronization of interventions at both local (provincial) and global (national) levels. A notable divergence exists between the empirical cumulative data and the modeled trajectory during the calibration phase in the provinces of Cabo Delgado and Nampula. These observations suggest that there is a certain heterogeneity in terms of the number of contacts that is not captured by the current model. In forthcoming investigations, it is advisable to examine ensemble methodologies and cross-validation techniques to further refine the model's precision in these provinces, in addition to exploring alternative mobility models and evaluating the ramifications of partial compliance with isolation protocols. Furthermore, the influence of heterogeneity in contact patterns across provinces necessitates additional scrutiny to enhance our comprehension of localized transmission dynamics.

The specification of precise model parameters represents an essential and often complex element of epidemiological modeling, particularly in situations that involve extensive datasets or newly emerging pathogens. These complexities emerge from a diverse array of factors, including data accessibility, variability, and the fundamental premises that are intrinsic to the modeling paradigm. For instance, parameters such as the basic reproduction number ($\mathcal{R}_0$), transmission coefficients, and recovery rates are frequently extracted from limited or incomplete datasets, consequently introducing a level of uncertainty [38]. The complexity intensifies in circumstances characterized by heterogeneous populations or adaptive interventions. For example, the execution of non-pharmaceutical strategies such as lockdowns alters contact patterns in manners that are challenging to quantify [39]. Similarly, real-time parameter estimation techniques such as Kalman filters, while effective, are heavily reliant on the quality and frequency of data updates, which may demonstrate significant variability across disparate regions [40]. In scenarios involving large datasets, computational limitations and challenges related to parameter identifiability often arise. Identifiability refers to the ability to uniquely estimate model parameters based on the available data, a condition that can be compromised in highly intricate models or when parameters display interdependencies [41]. This concern is particularly relevant in models that integrate mobility data, as evidenced in studies concerning COVID-19, where travel behaviors are heterogeneous and influenced by both voluntary actions and regulatory interventions [2]. Moreover, assumptions regarding seasonality, environmental factors, and population diversity can significantly influence the parameterization process. For example, the incorporation of seasonal forcing into models, as explored in the context of SARS-CoV-2, underscores the difficulties associated with accurately projecting long-term trends in the absence of robust data [41]. Future research endeavors should aim to address these challenges by leveraging advancements in data science, inclusive of machine learning methodologies, which possess the potential to enhance parameter estimation and model calibration. Furthermore, the advocacy for open data initiatives and standardized methodologies can alleviate uncertainty and strengthen reproducibility across various investigations. These strategies are essential for the refinement of epidemiological models and the assurance of their dependability in guiding public health policymaking.

In the realm of modeling the dynamics associated with infectious diseases, the accuracy of cumulative case data is critical for the effective estimation of parameters and the validation of predictive models. However, such data often face biases arising from a multitude of factors, including limitations in testing capacity, phenomena of underreporting, and delays linked to the reporting of cases. These obstacles are particularly pronounced in contexts marked by resource limitations, where the accessibility of diagnostic facilities and the promptness of data collection may prove to be inconsistent [42]. The capability for testing exhibits substantial heterogeneity across various geographical regions and temporal contexts, thereby affecting the identification and subsequent documentation of cases. For instance, in the early stages of the COVID-19 pandemic, the limited access to diagnostic tests led to considerable underreporting of cases in numerous low- and middle-income countries [43]. Such underreporting possesses the capacity to skew model outputs, ultimately resulting in the underestimation of infection rates and the postponement of peak identification in outbreaks. Moreover, delays in reporting, frequently attributable to logistical constraints or centralized public health systems, may introduce temporal inconsistencies that inaccurately represent the epidemic curve [44]. Furthermore, cumulative data inherently tends to smooth out temporal fluctuations, potentially obscuring the effects of short-term intervention strategies such as lockdowns or localized travel restrictions. For instance, a sudden reduction in reported cases, resulting from underreporting during weekends or holidays, may misleadingly suggest a decrease in transmission intensity, leading to ill-informed policy decisions [45]. To mitigate these limitations, modeling frameworks can be developed to account for reporting biases through the incorporation of correction factors or sensitivity analyses. Advanced statistical techniques, including Bayesian hierarchical models, possess the capability

to rectify acknowledged biases by integrating auxiliary datasets, such as excess mortality or syndromic surveillance data [46]. By recognizing and addressing these data-related obstacles, the robustness and applicability of epidemic models can be substantially improved, thus providing more reliable insights for public health interventions.

Our theoretical framework posits uniform contact rates within each province, thereby streamlining the computational methodology; however, this may inadequately reflect the intricacies inherent in actual transmission dynamics. In practice, contact rates exhibit considerable variability within provinces, influenced by factors such as population density, levels of urbanization, economic activities, and cultural practices [47, 48]. For example, urban regions typically demonstrate elevated contact rates as a consequence of denser populations and more frequent interpersonal interactions, in contrast to rural areas, which may present lower rates attributed to more dispersed populations and restricted mobility [49]. This presumption of homogeneity could yield skewed assessments of transmission dynamics, especially in provinces characterized by pronounced rural-urban disparities or significant socioeconomic diversity [50]. Neglecting to consider these intraprovincial discrepancies may culminate in an underappreciation of high-risk zones or an inflation of the perceived efficacy of interventions in regions with low population density. Enhancing this dimension of the model could necessitate the incorporation of spatially explicit data concerning population density, mobility trends, and socioeconomic indicators to formulate contact matrices specific to each region. Methodologies such as agent-based modeling (ABM) or network-based frameworks are particularly adept at capturing heterogeneous contact rates and their temporal fluctuations across more granular spatial dimensions [50]. Furthermore, utilizing high resolution mobility datasets, including those derived from mobile phone usage or transport systems, can furnish vital insights into local contact patterns [51]. Subsequent research endeavors should prioritize the integration of such heterogeneities to bolster the precision and detail of predictive analyses, particularly in contexts characterized by diverse demographic and geographic attributes. Acknowledging these variations will augment the applicability of models in formulating targeted interventions that effectively address localized transmission risks.

References

[1] S. A. Iyaniwura, N. Ringa, P. A. Adu, S. Mak, N. Z. Janjua, M. A. Irvine, and M. Otterstatter, "Understanding the impact of mobility on COVID-19 spread: A hybrid gravity-metapopulation model of COVID-19," *PLOS Computational Biology*, vol. 19, no. 5, p. e1011123, 2023. Available at: https://doi.org/10.1371/journal.pcbi.1011123

[2] M. Chinazzi, J. T. Davis, M. Ajelli, C. Gioannini, M. Litvinova, S. Merler, A. P. y Piontti, K. Mu, L. Rossi, K. Sun, C. Viboud, X. Xiong, H. Yu, M. E. Halloran, I. M. Longini, and A. Vespignani, "The effect of travel restrictions on the spread of the 2019 novel coronavirus (COVID-19) outbreak," *Science*, vol. 368, no. 6489, pp. 395–400, 2020. Available at: https://doi.org/10.1126/science.aba9757

[3] M. Zhang, S. Wang, T. Hu, X. Fu, X. Wang, Y. Hu, B. Halloran, Z. Li, Y. Cui, H. Liu, Z. Liu, and S. Bao, "Human mobility and COVID-19 transmission: a systematic review and future directions," *Annals of GIS*, vol. 28, no. 4, pp. 501–514, 2022. Available at: https://doi.org/10.1080/19475683.2022.2041725

[4] Y. Wei, J. Wang, W. Song, C. Xiu, L. Ma, and T. Pei, "Spread of COVID-19 in China: analysis from a city-based epidemic and mobility model," *Cities*, vol. 110, p. 103010, 2021. Available at: https://doi.org/10.1016/j.cities.2020.103010

[5] G. S. Costa, W. Cota, and S. C. Ferreira, "Outbreak diversity in epidemic waves propagating through distinct geographical scales," *Physical Review Research*, vol. 2, no. 4, p. 043306, 2020. Available at: https://doi.org/10.1103/PhysRevResearch.2.043306

[6] A. Arenas, W. Cota, J. Gómez-Gardeñes, S. Gómez, C. Granell, J. T. Matamalas, D. Soriano-Paños, and B. Steinegger, "Modeling the spatiotemporal epidemic spreading of COVID-19 and the impact of mobility and social distancing interventions," *Physical Review X*, vol. 10, no. 4, p. 041055, 2020. Available at: https://doi.org/10.1103/PhysRevX.10.041055

[7] R. K. Eisfeld and T. Just, "Urban density versus regional dispersion: On the risks in high-density conurbations in Germany during COVID-19," *Sustainable Cities and Society*, vol. 108, p. 105503, 2024. Available at: https://doi.org/10.1016/j.scs.2024.105503

[8] G. Pullano, L. G. Alvarez-Zuzek, V. Colizza, and S. Bansal, "Characterizing US spatial connectivity: implications for geographical disease dynamics and metapopulation modeling," *medRxiv*, pp. 2023–11, 2023. Available at: https://doi.org/10.1101/2023.11.22.23298916

[9] P. S. Peixoto, D. Marcondes, C. Peixoto, and S. M. Oliva, "Modeling future spread of infections via mobile geolocation data and population dynamics. An application to COVID-19 in Brazil," *PloS One*, vol. 15, no. 7, p. e0235732, 2020. Available at: https://doi.org/10.1371/journal.pone.0235732

[10] M. H. H. S. Uiterkamp, M. Gösgens, H. Heesterbeek, R. van der Hofstad, and N. Litvak, "The role of inter-regional mobility in forecasting SARS-CoV-2 transmission," *Journal of the Royal Society Interface*, vol. 19, no. 193, p. 20220486, 2022. Available at: https://doi.org/10.1098/rsif.2022.0486

[11] E. Prestige, P. Coletti, J. Backer, N. G. Davies, W. J. Edmunds, and C. I. Jarvis, "Estimating social contact rates for the COVID-19 pandemic using Google mobility and pre-pandemic contact surveys," *medRxiv*, pp. 2023–12, 2023. Available at: https://doi.org/10.1101/2023.12.19.23300209

[12] S. Flaxman, S. Mishra, A. Gandy, H. J. T. Unwin, T. A. Mellan, H. Coupland, C. Whittaker, H. Zhu, T. Berah, J. W. Eaton, M. Monod, P. N. Perez-Guzman, N. Schmit, L. Cilloni, K. E. C. Ainslie, M. Baguelin, A. Boonyasiri, O. Boyd, L. Cattarino, L. V. Cooper, Z. Cucunubá, G. Cuomo-Dannenburg, A. Dighe, B. Djaafara, I. Dorigatti, S. L. van Elsland, R. G. FitzJohn, K. A. M. Gaythorpe, L. Geidelberg, N. C. Grassly, W. D. Green, T. Hallett, A. Hamlet, W. Hinsley, B. Jeffrey, E. Knock, D. J. Laydon, G. Nedjati-Gilani, P. Nouvellet, K. V. Parag, I. Siveroni, H. A. Thompson, R. Verity, E. Volz, C. E. Walters, H. Wang, Y. Wang, O. J. Watson, P. Winskill, X. Xi, P. G. T. Walker, A. C. Ghani, C. A. Donnelly, S. Riley, M. A. C. Vollmer, N. M. Ferguson, L. C. Okell, and S. Bhatt, "Estimating the effects of non-pharmaceutical interventions on COVID-19 in Europe," *Nature*, vol. 584, no. 7820, pp. 257–261, 2020. Available at: https://doi.org/10.1038/s41586-020-2405-7

[13] G. Pullano, E. Valdano, N. Scarpa, S. Rubrichi, and V. Colizza, "Population mobility reductions during COVID-19 epidemic in France under lockdown," *MedRxiv*, vol. 29, p. 2020, 2020. Available at: https://www.epicx-lab.com/uploads/9/6/9/4/9694133/inserm-covid-19_report_mobility_fr_lockdown-20200511.pdf

[14] J. Arino and P. van den Driessche, "A multi-city epidemic model," *Mathematical Population Studies*, vol. 10, no. 3, pp. 175–193, 2003. Available at: https://doi.org/10.1080/08898480306720

[15] T. Dhirasakdanon, H. R. Thieme, and P. Van Den Driessche, "A sharp threshold for disease persistence in host metapopulations," *Journal of Biological Dynamics*, vol. 1, no. 4, pp. 363–378, 2007. Available at: https://doi.org/10.1080/17513750701605465

[16] A. Wesolowski, C. O. Buckee, K. Engø-Monsen, and C. J. E. Metcalf, "Connecting mobility to infectious diseases: the promise and limits of mobile phone data," *The Journal of Infectious Diseases*, vol. 214, no. suppl_4, pp. S414–S420, 2016. Available at: https://doi.org/10.1093/infdis/jiw273

[17] Z. Rapti, J. Cuevas-Maraver, E. Kontou, S. Liu, Y. Drossinos, P. G. Kevrekidis, M. Barmann, Q.-Y. Chen, and G. A. Kevrekidis, "The role of mobility in the dynamics of the COVID-19 epidemic in Andalusia," *Bulletin of Mathematical Biology*, vol. 85, no. 6, p. 54, 2023. Available at: https://doi.org/10.1007/s11538-023-01152-5

[18] MISAU. (2020) Coronovirus. Covid-19 boletins diário. Available at: https://www.misau.gov.mz/index.php/covid-19-boletins-diarios

[19] Z. Liu, P. Magal, O. Seydi, and G. Webb, "A COVID-19 epidemic model with latency period," *Infectious Disease Modelling*, vol. 5, pp. 323–337, 2020. Available at: https://doi.org/10.1016/j.idm.2020.03.003

[20] V. A. Karatayev, M. Anand, and C. T. Bauch, "Local lockdowns outperform global lockdown on the far side of the COVID-19 epidemic curve," *Proceedings of the National Academy of Sciences*, vol. 117, no. 39, pp. 24 575–24 580, 2020. Available at: https://doi.org/10.1073/pnas.2014385117

[21] S. He, S. Tang, and L. Rong, "A discrete stochastic model of the COVID-19 outbreak: Forecast and control," *Mathematical Biosciences and Engineering*, vol. 17, no. 4, pp. 2792–2804, 2020. Available at: http://doi.org/10.3934/mbe.2020153

[22] A. P. Masucci, J. Serras, A. Johansson, and M. Batty, "Gravity versus radiation models: On the importance of scale and heterogeneity in commuting flows," *Physical Review E – Statistical, Nonlinear, and Soft Matter Physics*, vol. 88, no. 2, p. 022812, 2013. Available at: https://doi.org/10.1103/PhysRevE.88.022812

[23] F. Simini, M. C. González, A. Maritan, and A.-L. Barabási, "A universal model for mobility and migration patterns," *Nature*, vol. 484, no. 7392, pp. 96–100, 2012. Available at: https://doi.org/10.1038/nature10856

[24] M. Tizzoni, P. Bajardi, A. Decuyper, G. Kon Kam King, C. M. Schneider, V. Blondel, Z. Smoreda, M. C. González, and V. Colizza, "On the use of human mobility proxies for modeling epidemics," *PLoS Computational Biology*, vol. 10, no. 7, p. e1003716, 2014. Available at: https://doi.org/10.1371/journal.pcbi.1003716

[25] P. C. Ventura, A. Aleta, F. A. Rodrigues, and Y. Moreno, "Modeling the effects of social distancing on the large-scale spreading of diseases," *Epidemics*, vol. 38, p. 100544, 2022. Available at: https://doi.org/10.1016/j.epidem.2022.100544

[26] L. Pappalardo, F. Simini, G. Barlacchi, and R. Pellungrini, "scikit-mobility: A python library for the analysis, generation and risk assessment of mobility data," *arXiv*, 2019. Available at: https://doi.org/10.48550/arXiv.1907.07062

[27] S. A. Pedro, F. T. Ndjomatchoua, P. Jentsch, J. M. Tchuenche, M. Anand, and C. T. Bauch, "Conditions for a second wave of COVID-19 due to interactions between disease dynamics and social processes," *Frontiers in Physics*, vol. 8, p. 574514, 2020. Available at: https://doi.org/10.3389/fphy.2020.574514

[28] A. Cassy, T. Marrufo, and S. Chicumbe, "COVID-19 em Moçambique, relatório do 1o ano, 2020-2021," Instituto Nacional de Saúde, Marracuene, Mozambique, Tech. Rep. 1, 2021. Available at: https://ons.nilzachipe.com/wp-content/uploads/2024/03/ONS-Relatorio-do-1o-Ano-da-COVID-19-Mocambique.pdf

[29] A. W. Byrne, D. McEvoy, A. B. Collins, K. Hunt, M. Casey, A. Barber, F. Butler, J. Griffin, E. A. Lane, C. McAloon *et al.*, "Inferred duration of infectious period of SARS-CoV-2: rapid scoping review and analysis of available evidence for asymptomatic and symptomatic COVID-19 cases," *BMJ Open*, vol. 10, no. 8, p. e039856, 2020. Available at: https://doi.org/10.1136/bmjopen-2020-039856

[30] T. Akiba, S. Sano, T. Yanase, T. Ohta, and M. Koyama, "Optuna: A next-generation hyperparameter optimization framework," in *Proceedings of the 25th ACM SIGKDD International Conference on Knowledge Discovery & Data Mining*, 2019, pp. 2623–2631.

[31] A. Saltelli, *Global Sensitivity Analysis: the Primer*, 1st ed. West sussexPO19 8SQ, England: John Wiley & Sons, 2008. Available at: https://www.andreasaltelli.eu/file/repository/A_Saltelli_Marco_Ratto_Terry_Andres_Francesca_Campolongo_Jessica_Cariboni_Debora_Gatelli_Michaela_Saisana_Stefano_Tarantola_Global_Sensitivity_Analysis_The_Primer_Wiley_Interscience_2008_.pdf

[32] J. Herman and W. Usher, "Salib: An open-source python library for sensitivity analysis," *Journal of Open Source Software*, vol. 2, no. 9, p. 97, 2017. Available at: https://doi.org/10.21105/joss.00097

[33] F. Gugole, L. E. Coffeng, W. Edeling, B. Sanderse, S. J. De Vlas, and D. Crommelin, "Uncertainty quantification and sensitivity analysis of COVID-19 exit strategies in an individual-based transmission model," *PLoS Computational Biology*, vol. 17, no. 9, p. e1009355, 2021. Available at: https://doi.org/10.1371/journal.pcbi.1009355

[34] D. A. Buch, J. E. Johndrow, and D. B. Dunson, "Explaining transmission rate variations and forecasting epidemic spread in multiple regions with a semiparametric mixed effects SIR model," *Biometrics*, vol. 79, no. 4, pp. 2987–2997, 2023. Available at: https://doi.org/10.1111/biom.13901

[35] M. U. G. Kraemer, C.-H. Yang, B. Gutierrez, C.-H. Wu, B. Klein, D. M. Pigott, L. du Plessis, N. R. Faria, R. Li, W. P. Hanage, J. S. Brownstein, M. Layan, A. Vespignani, H. Tian, C. Dye, O. G. Pybus, and S. V. Scarpino, "The effect of human mobility and control measures on the COVID-19 epidemic in China," *Science*, vol. 368, no. 6490, pp. 493–497, 2020. Available at: https://doi.org/10.1126/science.abb4218

[36] F. Pedregosa, G. Varoquaux, A. Gramfort, V. Michel, B. Thirion, O. Grisel, M. Blondel, P. Prettenhofer, R. Weiss, V. Dubourg, J. Vanderplas, A. Passos, D. Cournapeau, M. Brucher, M. Perrot, and E. Duchesnay, "Scikit-learn: Machine learning in python," *The Journal of Machine Learning Research*, vol. 12, pp. 2825–2830, 2011. Available at: https://www.jmlr.org/papers/volume12/pedregosa11a/pedregosa11a.pdf?ref=https:/

[37] P. Joaquim, D. Takahashi, and S. Pedro, "The role of interprovincial mobility in the dynamics of COVID-19 epidemic in mozambique: Insights from a stochastic metapopulation model," in *Anais do Encontro Nacional de Modelagem Computacional e Encontro de Ciência e Tecnologia de Materiais*, XXVII Encontro Nacional de Modelagem Computacional e XV Encontro de Ciência e Tecnologia dos Materiais. Ilhéus, Brasil: Even3, 2024. Available at: https://www.even3.com.br/anais/enmc2024/914710-the-role-of-interprovincial-mobility-in-the-dynamics-of-covid-19-epidemic-in-mozambique--insights-from-a-stochast

[38] N. C. Grassly and C. Fraser, "Mathematical models of infectious disease transmission," *Nature Reviews Microbiology*, vol. 6, no. 6, pp. 477–487, 2008. Available at: https://doi.org/10.1038/nrmicro1845

[39] J. M. Brauner, S. Mindermann, M. Sharma, D. Johnston, J. Salvatier, T. Gavenčiak, A. B. Stephenson, G. Leech, G. Altman, V. Mikulik, A. J. Norman, J. T. Monrad, T. Besiroglu, H. Ge, M. A. Hartwick, Y. W. Teh, L. Chindelevitch, Y. Gal, and J. Kulveit, "Inferring the effectiveness of government interventions against COVID-19," *Science*, vol. 371, no. 6531, p. eabd9338, 2021. Available at: https://doi.org/10.1126/science.abd9338

[40] F. Arroyo-Marioli, F. Bullano, S. Kucinskas, and C. Rondón-Moreno, "Tracking $\mathcal{R}$ of COVID-19: A new real-time estimation using the Kalman filter," *PloS One*, vol. 16, no. 1, p. e0244474, 2021. Available at: https://doi.org/10.1371/journal.pone.0244474

[41] R. A. Neher, R. Dyrdak, V. Druelle, E. B. Hodcroft, and J. Albert, "Impact of seasonal forcing on a potential SARS-CoV-2 pandemic," *medRxiv*, pp. 2020–02, 2020. Available at: https://doi.org/10.1101/2020.02.13.20022806

[42] A. H. Khan, *Challenges in Modeling of an Outbreak's Prediction, Forecasting and Decision Making for Policy Makers*. Singapore: Springer Singapore, 2021, pp. 377–408. Available at: https://doi.org/10.1007/978-981-16-2450-6_17

[43] K.-F. Chen, T.-W. Feng, C.-C. Wu, I. Yunusa, S.-H. Liu, C.-F. Yeh, S.-T. Han, C.-Y. Mao, D. Harika, R. Rothman, and A. Pekosz, "Diagnostic accuracy of clinical signs and symptoms of COVID-19: A systematic review and meta-analysis to investigate the different estimates in a different stage of the pandemic outbreak," *Journal of Global Health*, vol. 13, 2023. Available at: https://doi.org/10.7189/jogh.13.06026

[44] L. Ma, Z. Qiu, P. Van Mieghem, and M. Kitsak, "Reporting delays: A widely neglected impact factor in COVID-19 forecasts," *PNAS Nexus*, vol. 3, no. 6, 2024. Available at: https://doi.org/10.1093/pnasnexus/pgae204

[45] K. Gallagher, R. Creswell, D. Gavaghan, and B. Lambert, "Identification and attribution of weekly periodic biases in epidemiological time series data," *medRxiv*, pp. 2023–06, 2023. Available at: https://doi.org/10.1101/2023.06.13.23290903

[46] S. Engblom, R. Eriksson, and S. Widgren, "Bayesian epidemiological modeling over high-resolution network data," *Epidemics*, vol. 32, p. 100399, 2020. Available at: https://doi.org/10.1016/j.epidem.2020.100399

[47] K. Prem, A. R. Cook, and M. Jit, "Projecting social contact matrices in 152 countries using contact surveys and demographic data," *PLoS Computational Biology*, vol. 13, no. 9, p. e1005697, 2017. Available at: https://doi.org/10.1371/journal.pcbi.1005697

[48] A. Machens, F. Gesualdo, C. Rizzo, A. E. Tozzi, A. Barrat, and C. Cattuto, "An infectious disease model on empirical networks of human contact: bridging the gap between dynamic network data and contact matrices," *BMC Infectious Diseases*, vol. 13, pp. 1–15, 2013. Available at: https://doi.org/10.1186/1471-2334-13-185

[49] Y. Li, T. Hu, X. Gai, Y. Zhang, and X. Zhou, "Transmission dynamics, heterogeneity and controllability of SARS-CoV-2: a rural–urban comparison," *International Journal of Environmental Research and Public Health*, vol. 18, no. 10, p. 5221, 2021. Available at: https://doi.org/10.3390/ijerph18105221

[50] J. Chen, P. Bhattacharya, S. Hoops, D. Machi, A. Adiga, H. Mortveit, S. Venkatramanan, B. Lewis, and M. Marathe, "Role of heterogeneity: National scale data-driven agent-based modeling for the US COVID-19 scenario modeling hub," *Epidemics*, vol. 48, p. 100779, 2024. Available at: https://doi.org/10.1016/j.epidem.2024.100779

[51] A. L. Bertozzi, E. Franco, G. Mohler, M. B. Short, and D. Sledge, "The challenges of modeling and forecasting the spread of COVID-19," *Proceedings of the National Academy of Sciences*, vol. 117, no. 29, pp. 16 732–16 738, 2020. Available at: https://doi.org/10.1073/pnas.2006520117